quantities with a surprisingly good agreement with experiments. The potential is generally an improvement over the existing empirical ones.[1-3] By examining different potential expressions we have shown that both a quadrupole moment and an explicit treatment of hydrogens are important to obtain an acceptable functional agreement with quantum chemical data.

The reference interaction site model (RISM) has been used by Lowden and Chandler[20] and by Narten[18] in describing the structure of liquid benzene. Narten[18] made the conclusion that the best twelve-site RISM molecule gave a significantly better agreement with experimental X-ray results than that found for a six-site model. Since the gist of the RISM approach is the short-range repulsive interaction, this conclusion is an argument supporting the importance of an accurate description of the molecular extension. However, a twelve-site model has a drawback in simulations due to the large number of atom-atom interactions. In the case of benzene, this can partially be mastered by using a simplified potential at separations where the interaction in reality is isotropic. If the isotropic interaction is sufficiently small, a spherical cutoff[9] is an alternative way to reduce the number of interactions.

Solid benzene at low temperature may be characterized by both a high-translational and -orientational order, and molecules close to each other prefer a perpendicular orientation. At higher temperature the rotation about the C_6 axis tends to destroy the orientational order of the C_2 axes and averages out the previously pronounced atom-atom distribution function. In the liquid state there is only a small orientational correlation between two molecules except at very short distances where the anisotropic exchange repulsion favors the stacked configuration. This is, however, counteracted by the repulsive quadrupole-quadrupole interaction, and the stacked configuration at short separations is infrequent.

The small existing disagreement between experimental data and calculated results indicates that the quantum chemical calculated potential gives a slightly too small molecule and as a result a too attractive pair energy.

Other investigations[21] have shown that the quantum mechanical approach given by Karlström et al.[6] leads to molecular potentials where the exchange repulsion is slightly underestimated. This underestimate of the exchange repulsion is due to the lack of diffuse basis functions which gives a deeper interaction minimum at a shorter intermolecular distance.

These simulations are based on a pair potential. In order to improve a theoretical description of liquid and solid benzene, the many-body effect of the interaction has to be considered. Also, the classical treatment and the neglect of internal vibrations restrict the possible accuracy of the model.

Acknowledgment. Stimulating discussions with and valuable criticism of the manuscript by B. Jönsson, G. Karlström, B. Lindman, and H. Wennerström are gratefully acknowledged. Thanks are due to S. Linse for helpful program development. A grant from Stiftelsen Bengt Lundqvists Minne is also gratefully acknowledged.

Registry No. Benzene, 71-43-2.

(20) Lowden, L. J.; Chandler, D. *J. Chem. Phys.* **1974**, *61*, 5228.

(21) Karlström, G., private communication.

Electronic Structure and Optical Spectrum of *cis*-Diammineplatinum α-Pyridone Blue: Metal-Metal Bonding and Charge Transfer in a Four-Atom Pt(2.25) Chain

Alvin P. Ginsberg,*[1a] Thomas V. O'Halloran,[1b,c,d] Phillip E. Fanwick,*[1e] L. Steven Hollis,[1c] and Stephen J. Lippard*[1c,d]

Contribution from AT&T Bell Laboratories, Murray Hill, New Jersey 07974, the Department of Chemistry, University of Kentucky, Lexington, Kentucky 40506, the Department of Chemistry, Columbia University, New York, New York 10027, and the Department of Chemistry, Massachusetts Institute of Technology, Cambridge, Massachusetts 02139.
Received January 10, 1984

Abstract: Polarized single-crystal optical spectroscopy, together with a scattered wave Xα analysis, provides an understanding of the intriguing blue color and the metal-metal interactions in the Pt(2.25) chain complex *cis*-diammineplatinum α-pyridone blue (PPB), *cis*-$[Pt(NH_3)_2(C_5H_4NO)]_4(NO_3)_5 \cdot H_2O$. Pt-Pt bonding is found to be mainly due to σ overlap between Pt d_{z^2}, s hybrid orbitals. The net σ-bonding interaction between the end pairs of Pt atoms in the chain is stronger than between the middle pair. The PPB HOMO and LUMO are Pt-Pt σ^* in character and are delocalized over all four Pt atoms. Immediately below the HOMO are two orbitals with Pt-pyridone oxygen π^* character. These orbital characteristics are used to rationalize the redox chemistry of PPB. Of the unpaired spin density 94% is contained within the Pt spheres, with 43% in the two end spheres and 51% in the two inner spheres. PPB is therefore a Robin-Day class III-A compound. The observed [and calculated] optical transition energies (eV), intensities, and polarizations are as follows: ~1.55 vw, ? [1.63 w, x]; 1.82 s, z [1.50 s, z; 1.53 s, z; 2.14 s, z]; 2.25 vw, x [2.15 vw, x; 2.16 vw, x; 2.39 vw, x]; 2.58 m, z [2.80 s, z]; 2.69 wm, x [2.39 m, x]; 3.10 w, x [2.84 w, x; 3.10 w, x]. The blue color of PPB is due to the intense z-polarized transitions at 1.82 (680 nm) and 2.58 eV (480 nm). These may be described, respectively, as inner Pt-Pt bonding $\rightarrow$ inner Pt-Pt σ^* and outer Pt-Pt $\pi \rightarrow$ outer Pt-Pt σ^*. Both inner Pt $\rightarrow$ outer Pt and outer Pt $\rightarrow$ inner Pt charge transfer make important contributions to the intensity of the 680-nm band, while outer Pt $\rightarrow$ inner Pt charge transfer is the main contributor to the intensity of the 480-nm band.

Blue platinum complexes derived from the antitumor drug *cis*-diamminedichloroplatinum(II)[2] are of considerable current interest,[3] although they have been known for over a decade.[4] We previously reported the synthesis, X-ray crystal structure deter-

0002-7863/84/1506-5430$01.50/0

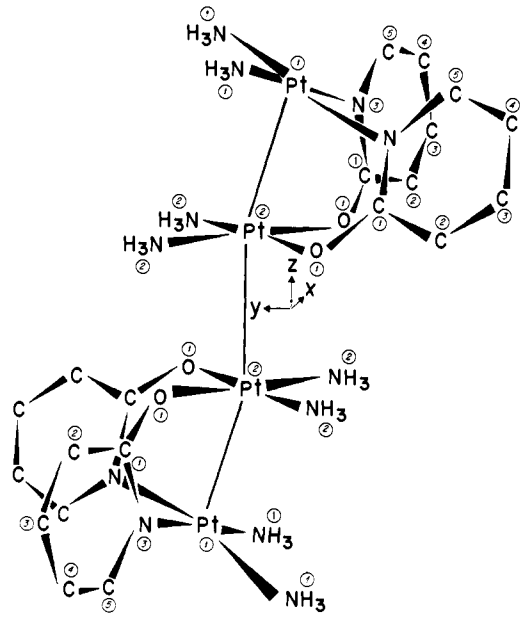

Figure 1. Structure of *cis*-diammineplatinum α-pyridone blue, $[Pt(NH_3)_2(C_5H_4NO)]_4^{5+}$, showing the numbering scheme and coordinate system used in the molecular orbital calculations. The origin of the coordinate system is at the midpoint of the Pt(2)–Pt(2) bond. Pyridone H atoms are omitted from the diagram for clarity.

mination, magnetic and single-crystal electron spin resonance spectral properties, and X-ray photoelectron spectrum of *cis*-diammineplatinum α-pyridone blue (PPB).[5] This mixed valence

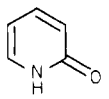

α-pyridone

compound, $[Pt(NH_3)_2(C_5H_4NO)]_4(NO_3)_5 \cdot H_2O$, has an amidate-bridged oligomeric structure with metal–metal bonding (Figure 1). Crystals of PPB are dark blue-black by reflected light. The color intensity and band position of the compound in aqueous solution are a sensitive function of anions, pH, temperature, and time,[5d] however, and of the matrix salt used to prepare pellets for solid-state absorption spectroscopy.[6] In order to identify the origin of the spectral transition(s) responsible for the intriguing blue color of this compound and to elucidate its electronic structure, especially the nature of the metal–metal interactions, we have carried out theoretical and polarized single-crystal optical spectroscopic studies on PPB. The present article reports the results of this work.

A first-principles theoretical analysis of the electronic structure of PPB offers considerable difficulty because of the large number of atoms in the cation (80), the low symmetry (C_{2h}), and the necessity of including relativistic corrections in the Pt valence levels in order to achieve realistic results.[7] The only feasible method at present appears to be a SCF–Xα–SW calculation.[8,9] On the basis of experience in interpreting the optical spectra of iridium complexes[10,11] and the optical spectra and metal–metal bonding in tungsten and rhenium dimers,[12,13] we anticipated that a relativistic SCF–Xα–SW calculation would facilitate assignment of the optical spectrum of PPB and would provide a useful description of the metal–metal bonding. As will be seen these expectations have been realized. The calculations provide an assignment of the optical spectrum in which the predicted polarizations, intensities, and energies of the transitions are in good agreement with experiment. Charge transfer from inner to outer and from outer to inner Pt atoms in the chain accounts for the intense bands in the optical spectrum and for the blue color of PPB. Of particular interest is the finding that there is a σ-bonding interaction between the outer pair of Pt atoms which does not occur between the inner pair. This difference provides an electronic reason for the shortness of the outer two Pt–Pt bonds compared to the middle bond in the chain. The calculation described in this paper was made possible by the availability of a Cray-1 supercomputer with reasonable overnight processing charges.

Experimental Section

Electronic spectra were recorded on a Cary 14 UV–visible spectrophotometer. The standard tungsten lamp was replaced with a DXN quartz halogen lamp. A Hamamatsu R928 photomultiplier tube was used in place of the standard tube.

Small (~0.5 mm on a side) platelike crystals of PPB, prepared as described previously,[5] were mounted with vacuum grease over pinholes punched in brass or stainless steel shim stock. There was no noticeable decomposition of the crystal on either mounting material after periods as long as 6 months. The plates were mounted in a Janis Super-varitemp cryostat. Temperature was controlled to ±1 K by a Lakeshore Cryogenics D7C temperature controller and silicon thermistor. Two Optics for Research PL-15 polarizers were used. Spectra were recorded with the polarizer in the sample compartment both in front and behind the crystal. The location of the polarizer made no difference in the spectrum. This polarizer was rotated by a crank running out of the sample compartment. A second polarizer was placed in the reference beam and set at the same angle as the sample polarizer to correct for any errors in the polarizers or optics.

Diffuse reflectance spectra were recorded with a Shamatsu reflectance attachment. The powders were stuck to a tape backing. Backgrounds for the tapes used were also recorded and subtracted out from the final spectra. The spectrum of $KMnO_4$ was recorded by using this procedure and agreed well with a previously reported spectrum.[14]

The crystal morphology was determined by indexing on an Enraf-Nonius CAD-4 diffractometer and studied by using a Huber Model 301 optical goniometer. Crystal thickness was measured by using the calibrated eyepiece on the optical goniometer.

Procedure for Calculations

SCF–Xα–SW calculations were carried out on a Cray-1 computer with revised versions[15] of the programs written originally by K. H. Johnson and F. C. Smith. Relativistic mass-velocity and Darwin corrections were applied by the method of Wood and Boring.[16]

(1) (a) AT&T Bell Laboratories. (b) Resident visitor, AT&T Bell Laboratories. (c) Columbia University. (d) Massachusetts Institute of Technology. (e) University of Kentucky.

(2) (a) Lippard, S. J. *Science (Washington, DC)* **1982**, *218*, 1075. (b) Barton, J. K.; Lippard, S. J. *Ann. N.Y. Acad. Sci.* **1978**, *313*, 686. (c) Lippard, S. J. *Acc. Chem. Res.* **1978**, *11*, 211.

(3) (a) Woollins, J. D.; Rosenberg, B. *Inorg. Chem.* **1982**, *21*, 1280. *J. Inorg. Biochem.* **1983**, *19*, 41. (b) Appleton, T. G.; Berry, R. D.; Hall, J. R. *Inorg. Chim. Acta* **1982**, *64*, L229. (c) Seul, M.; Neubacher, H.; Lohmann, W. *Z. Naturforsch B* **1981**, *36B*, 651. (d) Laurent, J.-P.; Lepage, P. *Can. J. Chem.* **1981**, *59*, 1083. (e) Matsumoto, K.; Fuwa, K. *J. Am. Chem. Soc.* **1982**, *104*, 897. (f) Laurent, J.-P.; Lepage, P.; Castan, P.; Arrizabalaga, P. *Inorg. Chim. Acta* **1982**, *67*, 31.

(4) (a) Shooter, K. V.; Howse, R.; Merrifield, R. K.; Robins, A. B. *Chem.-Biol. Interact.* **1972**, *5*, 289. (b) Hill, J. M.; Loeb, E.; MacLellan, A.; Hill, N. O.; Khan, A.; King, J. J. *Cancer Chemother. Rep.* **1975**, *59*, 647.

(5) (a) Barton, J. K.; Rabinowitz, H. N.; Szalda, D. J.; Lippard, S. J. *J. Am. Chem. Soc.* **1977**, *99*, 2827. (b) Barton, J. K.; Best, S. A.; Lippard, S. J.; Walton, R. A. *Ibid.* **1978**, *100*, 3785. (c) Barton, J. K.; Szalda, D. J.; Rabinowitz, H. N.; Waszczak, J. V.; Lippard, S. J. *Ibid.* **1979**, *101*, 1434. (d) Barton, J. K.; Caravana, C.; Lippard, S. J. *Ibid.* **1979**, *101*, 7269.

(6) Laurent, M. P.; Tewksbury, J. C.; Krogh-Jespersen, M.-B.; Patterson, H. *Inorg. Chem.* **1980**, *19*, 1656.

(7) The importance of relativistic corrections in electronic structure calculations on third transition period elements is reviewed in: Pitzer, K. S. *Acc. Chem. Res.* **1979**, *12*, 271. Pyykkö, P.; Desclaux, J. P. *Ibid.* **1979**, *12*, 276.

(8) Slater, J. C. "The Self-Consistent Field for Molecules and Solids: Quantum Theory of Molecules and Solids"; McGraw-Hill: New York, 1974; Vol. 4.

(9) Slater, J. C. "The Calculation of Molecular Orbitals"; Wiley: New York, 1979.

(10) Ginsberg, A. P.; Osborne, J. H.; Sprinkle, C. R. *Inorg. Chem.* **1983**, *22*, 254.

(11) Ginsberg, A. P.; Osborne, J. H.; Sprinkle, C. R. *Inorg. Chem.* **1983**, *22*, 1781.

(12) Cotton, F. A.; Hubbard, J. L.; Lichtenberger, D. L.; Shim, I. *J. Am. Chem. Soc.* **1982**, *104*, 679.

(13) Bursten, B. E.; Cotton, F. A.; Fanwick, P. E.; Stanley, G. C.; Walton, R. A. *J. Am. Chem. Soc.* **1983**, *105*, 2606.

(14) den Boef, G.; van der Beek, H. J.; Brauf, T. *Recl. Trav. Chim. Pays-Bas* **1958**, *77*, 1064.

(15) Locally modified version of the revision by M. Cook, B. Bursten, and G. Stanley.

(16) Wood, J. H.; Boring, A. M. *Phys. Rev. B: Solid State* **1978**, *18*, 2701.

Table I. Structure Parameters for *cis*-Diammineplatinum α-Pyridone Blue and for the C_{2h} Model Used in the Xα Calculation

parameter	crystal, C_i[a]	model, C_{2h}[a]
Pt(1)–Pt(2)	2.7745	2.7745
Pt(1)–N(1)	2.016, 2.041	2.026
Pt(1)–N(3)	2.033, 2.018	2.026
Pt(1)–Pt(2)–Pt(2)	164.6	164.6
N(1)–Pt(1)–N(1)	89.2	90.3
N(1)–Pt(1)–N(3)	88.9, 91.6	90.3
N(1)–Pt(1)–N(3)	176.1, 174.7	175.0
N(3)–Pt(1)–N(3)	89.9	88.7
Pt(2)–Pt(2)	2.8770	2.8770
Pt(2)–N(2)	2.024, 2.026	2.024
Pt(2)–O(1)	2.022, 2.016	2.019
N(2)–Pt(2)–N(2)	91.1	91.1
N(2)–Pt(2)–O(1)	88.0, 88.5	88.2
N(2)–Pt(2)–O(1)	178.3, 178.4	178.4
O(1)–Pt(2)–O(1)	92.4	92.3
O(1)–C(1)	1.32, 1.29	1.265
N(3)–C(1)	1.33, 1.35	1.31
C(1)–C(2)	1.40, 1.43	1.43
C(2)–C(3)	1.37, 1.36	1.37
C(3)–C(4)	1.40, 1.40	1.41
C(4)–C(5)	1.37, 1.36	1.36
C(5)–N(3)	1.36, 1.37	1.365
Pt(1)–N(3)–C(1)	123.0, 123.0	124.0
Pt(1)–N(3)–C(5)	115.5, 118.8	115.6
Pt(2)–O(1)–C(1)	122.8, 123.0	128.6[b]
C(1)–N(3)–C(5)	120.7, 118.0	119.4
O(1)–C(1)–N(3)[c]	120.9, 121.1	121.1
O(1)–C(1)–C(2)	118.0, 117.8	117.7
N(3)–C(1)–C(2)	121.1, 121.1	121.1
C(1)–C(2)–C(3)	118.4, 118.9	118.9
C(2)–C(3)–C(4)	120.3, 119.6	119.4
C(3)–C(4)–C(5)	118.5, 118.9	117.7
C(4)–C(5)–N(3)	120.8, 123.4	123.4
O(1)–N(3)[d]	2.30, 2.30	2.24
Pt(1)–Pt(1)–N(1)	101.3, 103.8	101.1
Pt(2)–Pt(1)–N(3)	81.4, 82.2	83.6
Pt(1)–Pt(2)–N(2)	100.5, 100.0	100.3
Pt(1)–Pt(2)–O(1)	81.4, 81.2	81.24
N(3)–C(1)–O(1)–Pt(2)	27.5, 19.2	12.4
tilt, τ[e]	28.12	26.2
twist, ω[f]	22.8	0.0

[a] Distances are in Å, angles in degrees. [b] A similar Pt(2)–O(1)–C(1) angle has been observed in the α-pyridonate bridged Pt(III) dimer. [c] The α-pyridonate bite angle. [d] The α-pyridonate bite distance. [e] The angle of inclination between the inner and outer ligand planes. [f] The twist angle between the inner and outer ligand planes.

Figure 1 shows the coordinate axes and atom numbering scheme that were used. The PPB cation in its crystal lattice has only C_i symmetry. The cation deviates from C_{2h} symmetry because of a 22° twist of the platinum coordination planes about the Pt(1)–Pt(2) bond axis.[5c] We idealized the molecule to C_{2h} symmetry by reducing the twist angle to 0°. It was also necessary to reduce the tilt angle between the platinum coordination planes by 2° in order to maintain the N,O bite distance of the α-pyridonate ligand. Table I summarizes the actual bond distances and angles in PPB and compares them with the corresponding values in our C_{2h} model; the model and the real PPB cation are in close agreement, and we believe that the small differences have no significant effect on the outcome of the calculation. Coordinates in atomic units (1 bohr = 0.52917 Å) were derived from the geometrical parameters listed in Table I for the C_{2h} model.

A set of overlapping atomic sphere radii was derived as follows.[17] For every bonded pair of atoms in the molecule, a pair of touching sphere radii was calculated by scaling the atomic number radii.[18] The different touching sphere radii calculated for a given atom were averaged to give an average touching sphere radius for the atom. Overlapping sphere radii were obtained by multiplying the average touching sphere radii by 1.303035; this factor was chosen to given 20% overlap between Pt(1) and Pt(2) spheres. The average of all sphere overlaps is ~25%, and the Pt(2)–Pt(2) sphere overlap is 16%. These sphere radii gave a satisfactory virial ratio ($-2T/V = 1.000253$ in the spin restricted nonrelativistic calculation) and were not further optimized. The outer sphere surrounding the cation was taken tangent to the outermost pyridone H sphere and was centered at the origin. A Watson sphere,[19] bearing a 5– charge and having the same radius and center as the outer sphere, was used to simulate the electrostatic interaction of the complex with its surrounding crystal lattice. Exchange-correlation parameter values (α) were taken from Schwarz's tables,[20,21] except for α_H for which the value recommended by Slater was used. In the extramolecular and intersphere regions α was taken as an average of the atomic sphere α values weighted by the number of valence electrons in the neutral atoms. Supplementary Table S1 summarizes the atomic coordinates, sphere radii, and α values used in the calculation.[22]

The initial cluster potential for PPB was constructed by superposing SCF–Xα charge densities for $Pt^{1.25+}$, C^0, N^0, O^0, and H^0. Partial waves through $l = 7$ in the extramolecular region, $l = 3$ in the Pt spheres, $l = 1$ in the C, N, and O spheres, and $l = 0$ in the H spheres were used to expand the wave functions. C_{2h} symmetry was used to factor the secular matrix. In the SCF calculations a weighted average of the initial and final potentials for a given iteration was used as the starting potential for the next iteration; the proportion of final potential in the average varied from 5% to 25%. The calculation was first converged in nonrelativistic spin restricted form (38 iterations). Relativistic corrections for the Pt core and valence levels were then slowly mixed into the potential over 10 iterations. After the relativistic calculation had converged (30 iterations) the potential was converted to spin-unrestricted form and the calculation was converged again. The spin-unrestricted relativistic calculation was considered to be converged after 25 iterations, when the largest change at any point in the potential was 0.0023 Ry and the valence levels had converged to ±0.0004 Ry or better. Each iteration required ~12 min of Cray-1 computer time.

The final spin-unrestricted ground-state potential was used to search for virtual levels up to a maximum energy of −0.200 Ry. This potential also served as the starting point for relativistic spin-unrestricted SCF calculations of the Slater transition states for one-electron transitions to the virtual levels.[8,9] These calculations were iterated until a plot of the transition energy vs. the change in the transition energy from one iteration to the next was linear for five successive points. The final value of the transition energy was obtained by extrapolating the plot to zero change in energy.

Results

Polarized Single-Crystal Spectra. *cis*-Diammineplatinum α-pyridone blue crystallizes in the triclinic space group $P\bar{1}$ with one formula per unit cell.[5c] The tetranuclear cation therefore occupies a site of symmetry $\bar{1}$. The spectra, however, will be analyzed in terms of the virtual C_{2h} symmetry used for the Xα calculation. The twofold axis in PPB is perpendicular to the Pt–Pt chain, and its projection onto the platinum coordination plane bisects the ammonia–platinum–O(α-pyridone) angle. In order to keep the local d_{z^2} orbitals pointing along the chain, this twofold axis will be designated the molecular x axis (Figure 1). Because point group C_{2h} only requires a plane perpendicular to the C_2 axis, the exact locations of the molecular y and z axes are not defined by the symmetry. This ambiguity creates some problems in analyzing the spectra. The platinum–platinum chain in PPB is not linear

(17) An attempt to use Norman's procedure[18] of taking the overlapping sphere radii as 88% of the atomic number radii led to zero overlap between the platinum spheres and over 50% overlap between N–H and C–H spheres.
(18) Norman, J. G. *Mol. Phys.* **1976**, *31*, 1191.
(19) Watson, R. E. *Phys. Rev.* **1958**, *111*, 1108.
(20) Schwarz, K. *Phys. Rev. B: Solid State* **1972**, *5*, 2466.
(21) Schwarz, K. *Theor. Chim. Acta* **1974**, *34*, 225.
(22) See the supplementary material paragraph at the end of the paper for details.

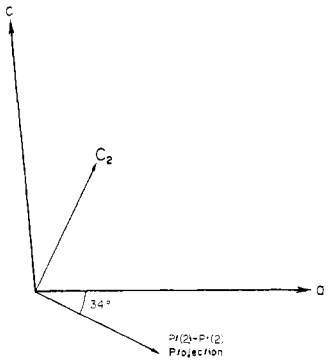

Figure 2. Relationship between the *a*–*c* plane and the projections of the Pt_4 chain as well as the approximate C_2 symmetry axis of *cis*-diammineplatinum α-pyridone blue (see text).

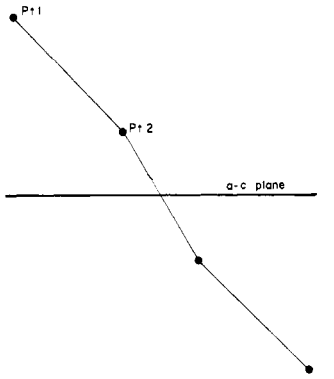

Figure 3. Relationships of Figure 2 rotated by 90°.

and is defined by two possible Pt–Pt vectors; however, even if the chain were linear the point group symmetry would be unchanged. Using the numbering system of Figure 1, we take the *z* axis to be the vector defined by the bond joining Pt(2) with Pt(2), to be consistent with the molecular orbital calculations.

The crystals used for spectroscopy were irregular, rectangular plates. Only the (010) face was thin enough to be studied. The long direction of the rectangle was determined to be the crystallographic *a* axis, in agreement with the previously reported morphology.[5c] When viewed under polarized light, the crystals displayed remarkable dichroism. Along one extinction direction the crystals were totally opaque, and no crystal was found which transmitted any light along this extinction direction. In the other direction the crystals appeared yellow-brown. In fact, only in reflected light do solid samples of PPB appear to be blue. Very thin sections (<10 μm) take on the yellow-brown color observed for light transmitted along the low polarization. The opaque extinction direction was found to lie 30 ± 4° off of the crystallographic *a* axis and 128 ± 4° away from the *c* axis.

The observed crystal optics are readily correlated with the crystal structure of *cis*-diammineplatinum α-pyridone blue. The projection of the Pt(2)–Pt(2) vector in the (010) face makes an angle of 34.4° with the *a* axis and an angle of 128.3° with the *c* axis. The opaque extinction direction for the (010) face is thus seen to lie along the projection of the platinum chain in this face. The molecular C_2 (*x*) axis is nearly in the *a*–*c* plane; the angle between the normal to (010) and this axis is 89.6°. These results are illustrated in Figures 2 and 3. The extinction direction normal to the Pt(2)–Pt(2) projection represents the molecular twofold rotation axis and should be totally devoid of any *z*-polarized components. If the alignment were not as favorable, bands observed when light is polarized along the *x* axis would be masked by the more intense components from the chain direction.

In order to gain information about those transitions polarized parallel to the platinum chain, the diffuse reflectance spectrum of a powdered sample was recorded. The spectrum is shown in Figure 4. There are two prominent peaks in this spectrum, a very broad peak at about 680 nm and one at 480 nm. These values

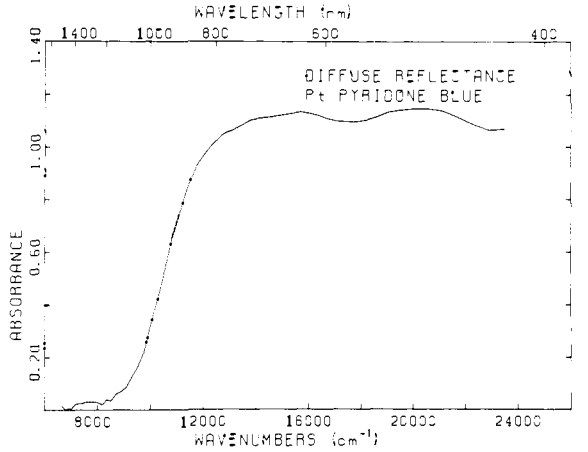

Figure 4. Diffuse reflectance spectrum of a powdered sample of *cis*-diammineplatinum α-pyridone blue at room temperature.

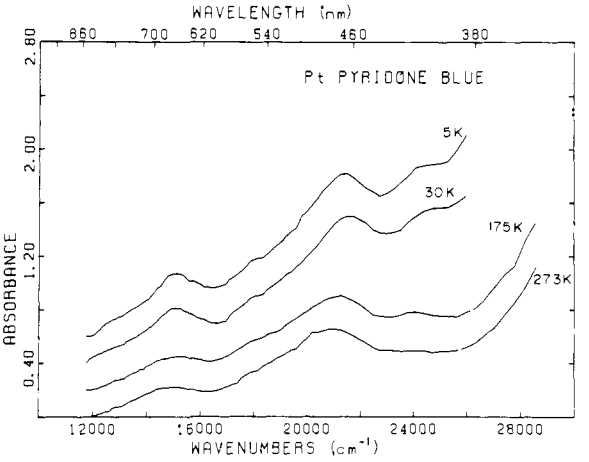

Figure 5. Spectrum of a single crystal of *cis*-diammineplatinum α-pyridone blue polarized along the molecular C_2 axis.

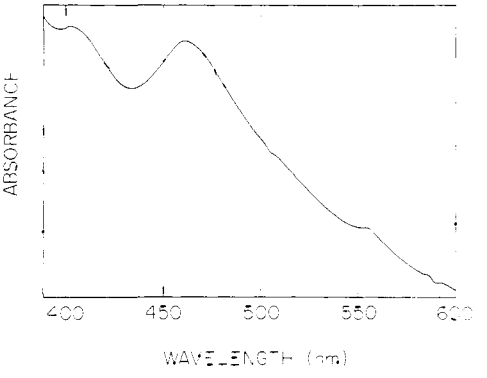

Figure 6. Spectrophotometer output of the 5 K spectrum of PPB. The ordinate is in arbitrary units with respect to zero.

agree with the previously reported solution spectra of *cis*-diammineplatinum α-pyridone blue in water[5d] and 0.1 M HNO_3.[6] No absorption was observed at wavelengths longer than ~1050 nm. A significant difference between the solid-state and solution spectra is the relative intensity of the two major features. Both in water and 0.1 M HNO_3 the band at 680 nm was 2–3 times as intense as the band at 480 nm, and this ratio varied with the platinum concentration. In the reflectance spectra they were of about equal intensity. It is presently uncertain whether this difference between the solid-state and solution spectra is real or due to solution equilibria effects.

A computerized plot of the crystal spectrum along the molecular C_2 axis at various temperatures is shown in Figure 5 while the actual output from the spectrophotometer for a sample at 5 K is displayed in Figure 6. The crystal used measured 20 ± 3 μm

thick. At room temperature the spectrum is dominated by the broad absorption at 460 nm. In very thin crystals this feature is the only one observed, while for thicker crystals a second band appears at 680 nm. Upon cooling, both of these bands become much sharper, and two weak features at 550 and 400 nm are revealed. The peak at 400 nm is first resolved at ~200 K while the feature at 550 nm only becomes observable below 30 K.

Molecular Orbital Calculations. Table II presents the calculated ground-state one-electron energies, charge distributions, and partial wave analyses for the upper valence molecular orbitals of PPB. The low-energy cutoff for Table II (−13.5 eV) is the lowest energy level in which there is metal–metal interaction; the table therefore includes all orbitals in which Pt–Pt interaction occurs. Valence levels with energies below −13.5 eV and core levels may be found in supplementary Tables S2 and S3. Additional virtual levels are given in supplementary Table S4. The basis function notation used in the tables and the discussion is explained in Table III. Figure 7 is a diagram of the energy levels in Table II. Wave function contour maps of selected orbitals are shown in Figures 8–10. Table V summarizes and compares the observed electronic absorptions and the calculated transition-state energies.

Discussion

Electronic Structure. The occupied valence molecular orbitals of *cis*-$[Pt(NH_3)_2(C_5H_4NO)]_4^{5+}$ have energies in the range −7.9 to −34 eV. Level 32 $b_u\uparrow$, the HOMO, is almost entirely localized on the Pt atoms, with somewhat more charge on Pt(2) than Pt(1); it is strongly Pt–Pt σ antibonding (Figure 8c). Immediately below the HOMO, in the interval −8.1 to −8.3 eV, there is a group of eight closely spaced levels which have most of their charge on the α-pyridone ligand; four of these levels, 32 $a_g\uparrow\downarrow$ and 31 $b_u\uparrow\downarrow$, also have appreciable metal character and show Pt–pyridone oxygen π^* interactions. Beginning at about −9.1 eV and extending to −13.5 eV is a group of 58 orbitals, of which 32 have greater than 50% metal character, 18 have 25–35% metal character, and the remaining 8 levels are essentially pure ligand orbitals. Included in this group are 30 orbitals in which there is significant metal–metal interaction; the main Pt–Pt σ-bonding orbital has the lowest energy in the group. The remaining orbitals in this group do not show significant interactions with Pt, being essentially nonbonding Pt and/or pyridone ligand orbitals (levels 22 b_g and 22 a_u also have considerable ammine nitrogen character). All of the important metal–ligand bonding orbitals occur below −13.5 eV and have not been included in Table II or Figure 7.

In addition to the occupied levels Table II includes 19 virtual levels with many more given in Table S4. The LUMO, 32 $b_u\downarrow$, is the most important of these; it has the same bonding characteristics as the HOMO (σ^*) and is the key orbital for understanding the optical spectrum, reduction, and coordination chemistry of PPB. Immediately above the LUMO are four levels which have most of their charge in the intersphere region; they are not important chemically nor are they important in the interpretation of the optical spectrum. The higher energy virtual orbitals in Table II are, with the exception of level 35 a_g, all metal–ligand antibonding in character. Orbital 35 a_g is the Pt(1)–Pt(2) and Pt(2)–Pt(2) $\sigma(p_z)$ bonding orbital. These levels are not involved in any of the observed optical transitions, nor do they play a role in the chemical behavior of PPB.

A notable feature of the results in Table II is the extent to which the Pt 6s and 6p atomic orbitals contribute to the MO's and also the extent to which the Pt atom d-orbital basis functions are mixed together. The mixing of the d-orbital functions is a consequence of the low symmetry and the zig-zag nature of the Pt chain. A recent extended Hückel calculation on a half PPB molecule, $[Pt_2(NH_3)_4(C_5H_4ON)_2]$, did not incorporate 6s and 6p Pt orbitals.[6] It led to the conclusion that the HOMO is the antibonding $d_{z^2}^-$ orbital and that immediately below the HOMO were most of the other metal d-orbitals. At still lower energy a group of ligand orbitals was found and then the metal–metal σ-bonding orbital $d_{z^2}^+$. The major difference between this ordering of the energy levels of PPB and what we have found by the Xα method is in the position of the d orbitals. As already mentioned (cf. Table II and Figure 7) the levels immediately below the HOMO are a group of α-pyridone ligand orbitals. The d orbitals occur beginning ~1 eV below this. As we shall see, this ordering leads to an assignment of the optical spectrum in good agreement with experiment.

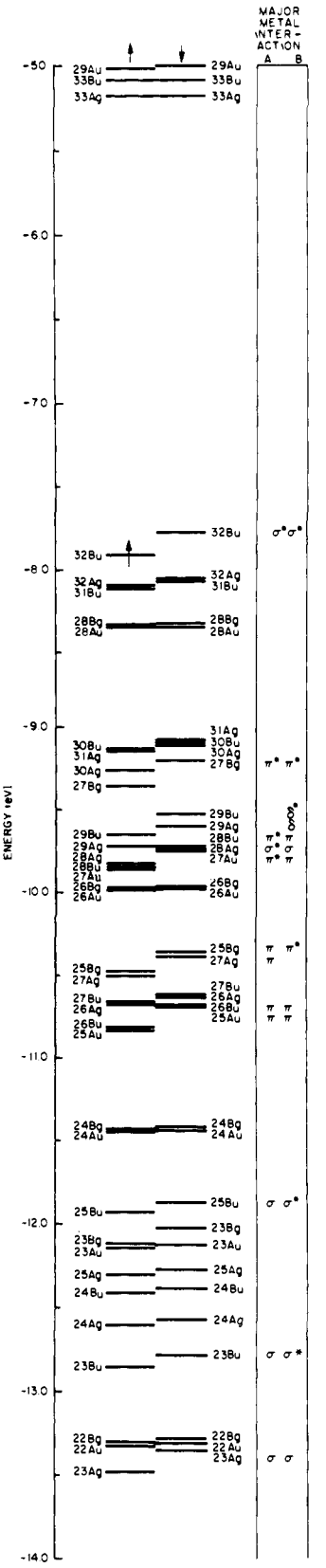

Figure 7. SCF valence energy levels for *cis*-diammineplatinum α-pyridone blue between −13.5 and −5.0 eV. The HOMO is level 32 $b_u\uparrow$. The metal–metal interactions under column A are Pt(1)–Pt(2), those under column B are Pt(2)–Pt(2).

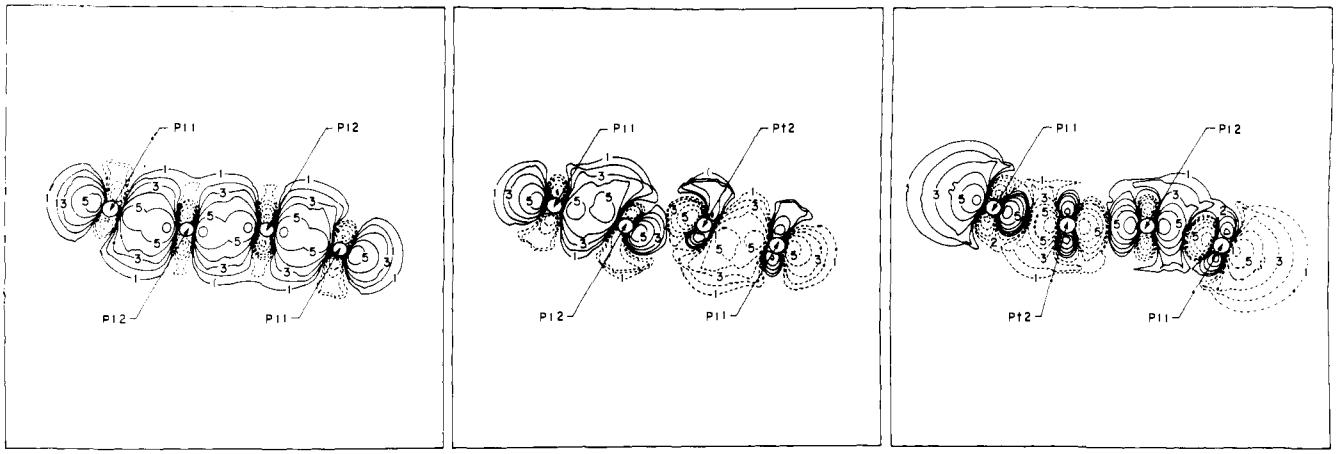

Figure 8. Wave function contour maps of orbitals with strong σ interactions. Plots are in the *yz* plane. Solid and broken lines denote contours of opposite sign having magnitudes indicated by the numerical labels: 1, 2, 3, 4, 5, 6 = 0.005, 0.010, 0.020, 0.04, 0.08, 0.160 $(e/bohr^3)^{1/2}$. Contours close to atomic centers are omitted for clarity. (left) Orbital 23 a_g. (center) Orbital 23 b_u. (right) Orbital 32 $b_u\uparrow$. The map of the LUMO, orbital 32 $b_u\downarrow$, is essentially the same.

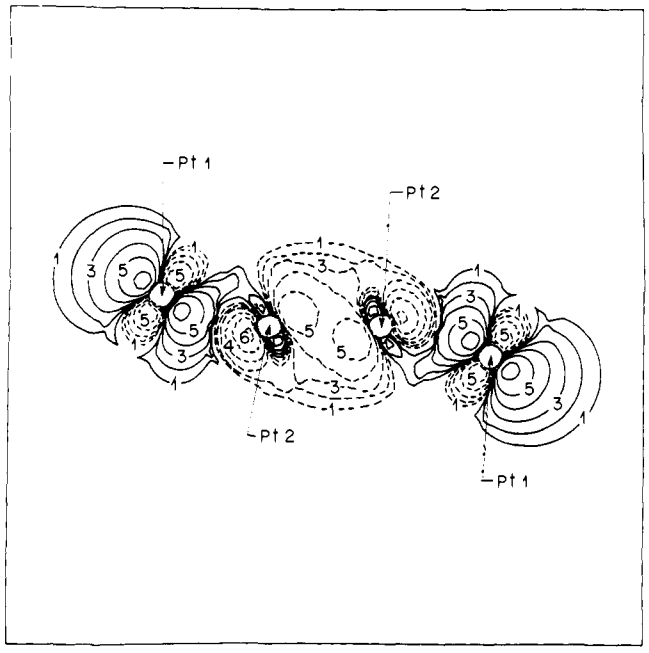

Figure 9. *yz*-Plane wave function contour map of orbital 28 a_g, the originating orbital for the 680 nm transition. Contour magnitudes and sign convention are as in Figure 8.

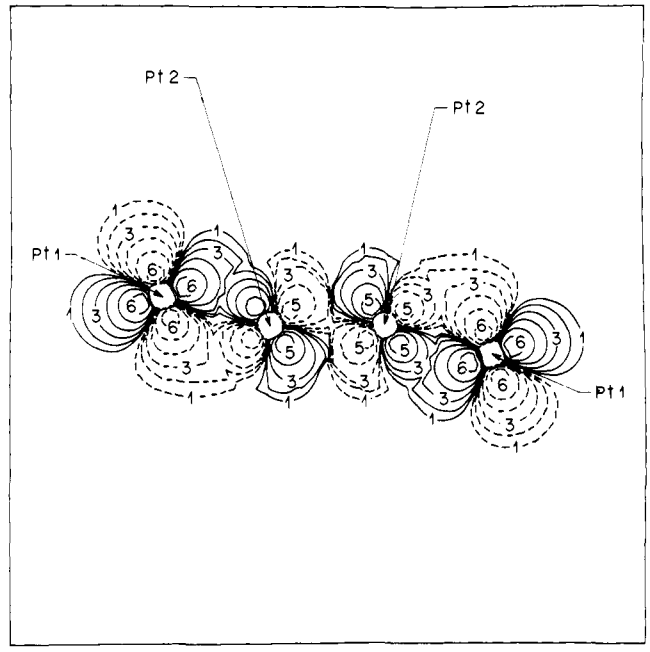

Figure 10. *yz*-Plane wave function contour map of orbital 27 a_g, the originating orbital for the 480-nm transition. Contour magnitudes and sign convention are as in Figure 8.

Metal–Metal Bonding. Table IV summarizes the orbitals in which significant metal–metal interaction occurs. A qualitative description of the interactions in each orbital, as deduced from wave function contour maps and the nature of the basis functions contributing to the orbital, is also given in the table.

σ-Bonding in orbitals 23 a_g and 23 b_u is by far the most important Pt–Pt interaction in the complex. In orbital 23 a_g, Figure 8a, there is strong Pt(1)–Pt(2) and Pt(2)–Pt(2) bonding which occurs via overlap of $d_{z^2}^+$, s^+ hybrid orbitals; the hybrids on the Pt(1) atoms also contain significant amounts of d_{yz}^+ and $d_{x^2-y^2}^+$. In orbital 23 b_u, Figure 8b, there are moderately strong Pt(1)–Pt(2) bonding and Pt(2)–Pt(2) antibonding interactions. In this case the σ overlap takes place between a $d_{z^2}^-$, s^-, d_{yz}^-, p_z^+ hybrid on Pt(1) and a d_{yz}^-, p_y^+, $d_{z^2}^-$, p_z^+, s^- hybrid on Pt(2). The bonding interaction in orbital 23 $a_g\uparrow$ is effectively canceled out by the σ* interaction in orbital 32 $b_u\uparrow$ (Figure 8), which is strongly Pt(1)–Pt(2) and Pt(2)–Pt(2) antibonding. It is the uncanceled interaction in orbital 23 $a_g\downarrow$, as well as the interaction in orbital 23 b_u, which provides the σ bonds between the Pt atoms in PPB. Since orbital 23 a_g contributes essentially equally to the Pt(1)–Pt(2) and Pt(2)–Pt(2) bonds, while orbital 23 b_u makes a bonding contribution only to the Pt(1)–Pt(2) bond, it is clear that the Pt(1)–Pt(2) σ bond must be stronger than the Pt(2)–Pt(2) σ bond. This result is consistent with the fact that the Pt(1)–Pt(2) bond length (2.779 Å) is shorter than the Pt(2)–Pt(2) bond length (2.885 Å).[5c] The presence of a Pt(1)–Pt(2) σ-bonding interaction which is not canceled when the σ-antibonding LUMO 32 $b_u\downarrow$ is occupied accounts for the fact that in the reduced complex, $[Pt_2(NH_3)_4(C_5H_4NO)_2]_2(NO_3)_4$, the Pt(1)–Pt(2) distance (2.877 Å) is much shorter than the Pt(2)–Pt(2) distance (3.129 Å)[23] and is similar to the Pt–Pt distance in the partially oxidized linear chain complex $K_2[Pt(CN)_4]Br_{0.3}$.[24] In the latter compound, the partial oxidation reduces the σ antibonding charge and gives a weak σ bond and a Pt–Pt distance of 2.890 Å.

In addition to the σ interactions there are weak uncompensated π interactions that contribute to the Pt–Pt bonding. As may be seen from Table IV the π interactions in PPB are spread over a number of orbitals; the interactions in each orbital are weak, and no single orbital makes a predominant contribution. Most of the π interactions are canceled by approximately equivalent π* interactions, except for the bonding interactions in orbitals 26 b_u

(23) Hollis, L. S.; Lippard, S. J. *J. Am. Chem. Soc.* **1983**, *105*, 3494.
(24) Krogmann, K.; Hausen, H. D. *Z. Anorg. Allg. Chem.* **1968**, *358*, 67.

Table II. Upper Valence Molecular Orbitals of $[Pt(NH_3)_2(C_5H_4NO)]_4^{5+}$

C_{2h} level	energy, eV ↑	energy, eV ↓	relative charge distribution, %[b,c] 2Pt(1)	2Pt(2)	4N(1)	4N(3)	4N(2)	4O(1)	4C(1)	4C(2)	4C(3)	4C(4)	4C(5)	basis functions[d] 2Pt(1)	2Pt(2)	intersphere charge
35 a_g	−4.45	−4.44	36	40	2	3	1	1	2	4	5	0	5	p_z^-, p_y^-, d_{yz}^+	p_z^-	24
31 a_u	−4.58	−4.50	62	1	11	13	0	1	2	3	4	0	3	d_{xy}^-, d_{xz}^-		10
30 b_g	−4.66		61	4	11	11	2	1	1	1	3	0	3	d_{xy}^+, d_{xz}^+		34
30 b_g		−4.60	53	13	9	9	4	2	1	1	3	0	3	d_{xy}^+, d_{xz}^+	d_{xy}^+	39
34 a_g	−4.73	−4.73														91
30 a_u	−4.88	−4.78	3	68	1	0	15	11	1	1	0	0	0		d_{xy}^-	27
29 b_g	−5.00	−4.88	0	72	0	0	15	11	1	1	0	0	0		d_{xy}^+	14
29 a_u	−5.02	−5.00	2	64	1	2	11	13	0	2	2	0	1		d_{xy}^-	69
33 b_u	−5.09	−5.09														96
33 a_g	−5.19	−5.19														96
32 b_u		−7.77	42	52	1	1	1	1	0	0	0	1	0	$d_{z^2}^-$, d_{yz}^-, p_z^+	$d_{z^2}^-$, s^-	6
32 b_u	−7.91		41	50	0	1	1	2	0	1	0	1	1	$d_{z^2}^-$, d_{yz}^-, p_z^+	$d_{z^2}^-$, s^-	6
32 a_g	−8.10	−8.06	9	17	0	9	0	19	5	15	0	19	7		$d_{x^2-y^2}^+$	22
31 b_u	−8.11	−8.07	10	19	0	8	0	18	5	14	0	17	7	$d_{x^2-y^2}^-$, d_{yz}^-	$d_{x^2-y^2}^-$, $d_{z^2}^-$	21
28 b_g	−8.33	−8.32	0	1	0	5	0	15	9	25	1	27	17			30
28 a_u	−8.33	−8.33	0	0	0	5	0	15	9	26	0	27	17			30
31 a_g		−9.07	44	21	1	7	0	1	0	10	7	0	9	$d_{x^2-y^2}^+$, $d_{z^2}^+$, d_{yz}^+	d_{yz}^+, $d_{x^2-y^2}^+$	14
30 b_u	−9.14	−9.08	50	3	1	11	0	0	0	13	11	0	11	$d_{x^2-y^2}^-$, d_{yz}^-		18
30 a_g		−9.11	33	54	0	3	1	1	0	3	2	0	2	$d_{x^2-y^2}^+$, $d_{z^2}^+$	d_{yz}^+	6
31 a_g	−9.14		50	3	1	11	0	0	0	13	11	0	11	$d_{x^2-y^2}^+$, d_{yz}^+		17
27 b_g	−9.36	−9.21	19	73	0	0	1	4	1	0	0	0	0	d_{xz}^+, d_{xy}^+	d_{xz}^+	2
30 a_g	−9.26		28	67	0	1	1	1	0	0	0	0	0	$d_{z^2}^+$, $d_{x^2-y^2}^+$	d_{yz}^+	2
29 b_u	−9.72	−9.52	13	67	0	1	1	3	5	0	2	5	2	$d_{x^2-y^2}^-$, $d_{z^2}^-$	$d_{x^2-y^2}^-$	8
29 a_g	−9.72	−9.60	11	67	0	1	1	5	6	0	2	5	2	$d_{x^2-y^2}^+$, $d_{z^2}^+$, d_{yz}^+	$d_{x^2-y^2}^+$	9
28 a_g	−9.83	−9.72	51	39	0	0	0	5	1	0	0	1	1	d_{yz}^+, s^+, $d_{z^2}^+$	$d_{z^2}^+$, p_z^-, d_{yz}^+, $d_{x^2-y^2}^+$	5
28 b_u	−9.85	−9.72	50	44	1	0	1	1	1	0	0	1	1	$d_{z^2}^-$, d_{yz}^-	d_{yz}^-, $d_{x^2-y^2}^-$	4
27 a_u	−9.86	−9.73	56	39	1	1	0	1	1	0	0	0	0	d_{xz}^-, d_{xy}^-	d_{xz}^-	3
26 b_g	−9.97	−9.96	1	1	0	31	0	1	0	20	33	10	1			29
26 a_u	−9.97	−9.96	0	2	0	31	0	1	0	20	33	10	1			29
25 b_g	−10.47	−10.35	75	15	1	1	1	5	0	0	0	0	0	d_{xz}^+, d_{xy}^+	d_{xz}^+	3
27 a_g	−10.50	−10.38	70	18	1	0	1	7	0	0	0	0	0	$d_{z^2}^+$, d_{yz}^+, $d_{x^2-y^2}^+$	d_{yz}^+	3
27 b_u	−10.65	−10.62	33	4	0	4	0	1	0	14	24	16	3	$d_{x^2-y^2}^+$, d_{yz}^+		25
26 a_g	−10.66	−10.62	33	2	1	4	0	0	0	15	25	16	2	$d_{x^2-y^2}^+$		26
26 b_u	−10.82	−10.69	44	47	1	0	1	4	0	1	1	0	0	d_{yz}^-, $d_{x^2-y^2}^-$, $d_{z^2}^-$	d_{yz}^-	5
25 a_u	−10.82	−10.70	40	48	1	0	1	8	1	0	0	0	0	d_{xz}^-, d_{xy}^-	d_{xz}^-	4
24 b_g	−11.42	−11.42	0	2	0	18	2	46	1	1	5	10	14			21
24 a_u	−11.43	−11.43	0	2	1	19	2	45	0	1	5	10	14			21
25 b_u	−11.93	−11.86	33	27	0	2	5	29	1	1	0	0	0	d_{yz}^-, $d_{z^2}^-$, s^-	$d_{z^2}^-$, p_y^+, s^-	1
23 b_g	−12.12	−12.09	3	19	2	11	9	36	5	7	2	2	3		p_x^-, d_{xz}^+	7
23 a_u	−12.14	−12.12	3	17	2	10	9	39	5	7	2	2	3		p_x^+, d_{xz}^-	7
25 a_g	−12.30	−12.26	11	19	3	14	11	32	1	1	1	2	5	$d_{x^2-y^2}^+$, d_{yz}^+, $d_{z^2}^+$	p_y^-, d_{yz}^+, $d_{x^2-y^2}^+$	10
24 b_u	−12.41	−12.37	19	15	5	23	2	22	0	0	1	3	8	$d_{x^2-y^2}^-$, $d_{z^2}^-$, p_y^+, s^-	$d_{x^2-y^2}^-$, $d_{z^2}^-$	13
24 a_g	−12.60	−12.56	7	23	4	13	5	31	4	5	1	2	4		p_y^-, $d_{x^2-y^2}^+$, d_{yz}^+, $d_{z^2}^+$	7
23 b_u	−12.85	−12.78	25	31	1	4	5	21	4	5	1	1	1	$d_{z^2}^-$, s^-, d_{yz}^-, p_z^+	d_{yz}^-, p_y^+, $d_{z^2}^-$, p_z^+, s^-	0
22 b_g	−13.30	−13.28	22	2	28	15	2	15	3	1	0	2	4	p_x^-		0
22 a_u	−13.31	−13.29	22	2	28	15	1	17	3	1	0	2	4	p_x^+		0
23 a_g	−13.47	−13.35	32	64	0	1	0	1	0	0	0	0	0	$d_{z^2}^+$, s^+, $d_{x^2-y^2}^+$, d_{yz}^+	$d_{z^2}^+$, s^+	0

[a] The highest occupied level is 32 b_u↑. [b] Relative percentage of the total population of the level located within the indicated region, $\sum_{\text{atomic spheres}}$ (relative atomic sphere charges) = 100%. The intersphere charge is shown in the last column of the table; the outersphere charge was small in all cases. For levels with very large intersphere charge, the relative atomic sphere charge distribution is not given. 2Pt(1) refers to the combined Pt(1) atomic spheres, 2Pt(2) to the combined Pt(2) spheres, etc. The ammine and pyridone H spheres are omitted from the table. [c] For most of the levels, the spin-up (↑), spin-down (↓), and spin-restricted charge distributions are essentially the same; the spin-restricted values are given in the table for these levels. In the few instances where spin-up and spin-down levels have significantly different charge distributions (due to mixing with nearby levels), they are listed separately with the appropriate spin unrestricted charge distribution. [d] When more than 10% of the population of a level is located within the Pt(1) or Pt(2) spheres, the spherical harmonic basis functions contributing more than 10% of the charge in that region are listed in order of decreasing importance. See Table III for an explanation of the basis function notation.

Table III. 2Pt(1) and 2Pt(2) Spherical Harmonic Basis Functions for C_{2h} *cis*-$[Pt(NH_3)_2(C_5H_4NO)]_4^{5+}$

representation	2Pt(1) or 2Pt(2) functions[a]
A_g	s^+, p_y^-, p_z^-, $d_{z^2}^+$, $d_{x^2-y^2}^+$, d_{yz}^+
B_g	p_x^-, d_{xy}^+, d_{xz}^+
A_u	p_x^+, d_{xy}^-, d_{xz}^-
B_u	s^-, p_y^+, p_z^+, $d_{z^2}^-$, $d_{x^2-y^2}^-$, d_{yz}^-

[a] The basis functions are represented by the constitutent atomic orbital symbols with a superscript + or − to indicate, respectively, a sum or difference combination of orbitals on two symmetry-related atoms. Thus, $p_y^-(Pt(2)) = 1/(2)^{1/2}[p_y(Pt(2)) - p_y(Pt(2'))]$, etc.

and 28 b_u. There are also weak uncompensated Pt–Pt bonding and antibonding interactions, neither π nor σ in character, in orbitals 30 a_g and 31 $a_g\downarrow$. Overall, the major effect of these weak interactions is to enhance the Pt(2)–Pt(2) bond, possibly by enough to nullify the Pt(2)–Pt(2) σ^* interaction in orbital 23 b_u. The only essentially pure δ-bonding interaction which we were able to identify occurs between the inner Pt atoms in orbital 29 a_g and is canceled by a corresponding δ^* interaction in orbital 29 b_u. A δ interaction between Pt(1) and Pt(2) was not found.

Assignment of the Optical Spectrum. Table V summarizes the observed electronic absorptions and assignments for the $[Pt(NH_3)_2(C_5H_4N)]_4^{5+}$ cation. The assignments were made by associating with each absorption the one-electron transition(s) which is (are) in best agreement with it in regard to energy, intensity, and polarization. Transition intensities were estimated qualitatively by decomposing each transition into component transitions between the basis functions comprising the initial and terminal MO's. The transition intensity was then assigned according to the following rules: (1) A dipole-allowed transition is called "strong" if it has an important interatomic charge transfer component between orbitals well directed for interaction. If the orbitals are poorly directed for interaction the transition is called "medium". (2) A dipole-allowed transition which owes its intensity to intraatomic d–d transitions is called "weak". (3) A dipole-forbidden, vibronically allowed transition is called "very weak".

As may be seen from Table V the agreement between observed and calculated spectra is good. Nearly all of the absorptions are assigned as dipole-allowed, spin-allowed[25] transitions which terminate in the LUMO, level 32 $bu\downarrow$; only the very weak *x*-polarized 550-nm band is attributed to dipole-forbidden vibronically allowed transitions. Aside from the absorption at 460 nm, which corresponds to ligand → metal charge transfer, all of the dipole-allowed bands are accounted for as transitions between MO's centered overwhelmingly on the metal atoms.

The strongest absorption observed in the spectrum of PPB is a broad *z*-polarized band centered at 680 nm. This band is assigned to the group of strong intensity transitions predicted in the range from 1.50 to 2.14 eV (Table V). An important contributor is the transition from orbital 28 $a_g\downarrow$ to the LUMO, which owes its intensity to the metal–metal charge-transfer component Pt(2) $d_{z^2}^+$, p_z^- → Pt(1) $d_{z^2}^-$, p_z^+. Since orbital 28 a_g (Figure 9) is σ bonding between the inner pair of Pt atoms and σ antibonding between the outer pairs while the LUMO (Figure 8, right) is σ antibonding between both inner and outer Pt atom pairs, this transition may be described as Pt(2)–Pt(2) σ → Pt(2)–Pt(2) σ^*. Important contributions to the 680-nm band also come from transitions 31 $a_g\downarrow$ → 32 $b_u\downarrow$ and 30 $a_g\downarrow$ → 32 $b_u\downarrow$, both of which owe their intensity to the charge-transfer component Pt(1) $d_{z^2}^+$ → Pt(2) $d_{z^2}^-$. Both of these transitions may also be described, approximately, as Pt(2)–Pt(2) bonding → Pt(2)–Pt(2) σ^*. All of the transitions which contribute to the 680-nm band are therefore characteristic of the tetrameric structure of PPB. Since analogous transitions are not possible in a dimer, EHMO calculations on a dimer model for the tetramer[6] inevitably failed to reveal these assignments for the 680-nm band.

From the thickness of the PPB crystals that were examined and their failure to transmit *z*-polarized light, we estimate $\epsilon_{680} > 4000$ M^{-1} cm^{-1}. A 1.0×10^{-4} M solution of PPB in 0.1 M HNO_3 has $\epsilon_{680} = 2580$ M^{-1} cm^{-1} about 15 min after mixing; 15 min later its extinction is 5% less. The much smaller values previously reported for ϵ_{680} in aqueous solution[5d] are attributed to extensive disproportionation of the tetramer into α-pyridonate-bridged Pt(II) and Pt(III) dimers. This reaction is repressed by nitrate ion and promoted by halide ions, which are proposed to stabilize the Pt(III) cations $[Pt_2(NH_3)_4(C_5H_4NO)_2X_2]^{2+}$.[5d]

A weak 680-nm band is also observed in the *x*-polarized spectrum of PPB; we assign it to the same transitions as the *z*-polarized band. When the known crystal concentration of 1.65 M and the observed thickness of 0.002 cm are used, the molar absorptivity is only about 120 M^{-1} cm^{-1}. The presence of this forbidden component in the polarization perpendicular to the chain may be accounted for by three possible mechanisms, all of which probably make some contribution to its intensity. (1) In our analysis we have idealized the molecular symmetry from C_i to C_{2h}. Under C_i symmetry the *x* components of the transitions which give rise to the 680-nm (*y*,*z*) band are all allowed and should appear as one or more weak absorptions. (2) A slight misalignment of the transition moment vector and the crystal extinction direction will enhance the *x*-component intensity. Since the crystals belong to a triclinic space group this possibility is a real one. If a value for the molar absorptivity of 4000 M^{-1} cm^{-1} is assumed, then a change in the alignment of the transition moment of less than 1° would more than account for the observed intensity. This deviation would be hard to measure accurately using the polarizing microscope owing to the difficulty in locating the crystal axes in the irregular crystals. (3) The absorption might also arise from a vibronic component that has a polarization along the molecular *x* axis. The fact that the band narrows and increases in intensity upon cooling does not rule out the vibronic assignment; it only suggests that the coupling vibration has a frequency greater than kT.

After the 680-nm band the next strongest absorption found in the spectrum of PPB occurs at 480 nm and is *z*-polarized. We assign this band to the transition from orbital 27 $a_g\downarrow$ to the LUMO. Its intensity derives from the metal–metal charge-transfer component Pt(1) $d_{z^2}^+$ → Pt(2) $d_{z^2}^-$. Since orbital 27 a_g (Figure 10) is π bonding between the outer pairs of Pt atoms and effectively nonbonding between the inner Pt atom pair, the 480-nm transition may be described as Pt(1)–Pt(2) π → Pt(1)–Pt(2) σ^*. This transition is accompanied by significant electron delocalization since in orbital 27 a_g 70% of the charge resides in the Pt(1) sphere while the LUMO has 42% of its charge on Pt(1) and 52% on Pt(2). Unlike the 680-nm transition, the 480-nm transition does not require the tetrameric structure of PPB. An analogous absorption, shifted in energy of course, is to be expected for a Pt(III) or Pt(2.5) dimer of similar structure. This interpretation is consistent with the results of a spectrophotometric study of the decomposition of aqueous solutions of PPB.[5d] It was found that on standing the 680-nm band slowly disappears while, simultaneously, the 480-nm band gradually shifts to higher energy and increases in intensity. We have ascribed this behavior to the disportionation reaction mentioned previously.[2a] Neither the Pt(II) nor the Pt(III) dimers which are formed can have a band analogous to the 680-nm absorption of the tetramer. A band corresponding to the 480-nm tetramer transition is expected for the Pt(III) or Pt(2.5) but not for the Pt(II) dimer. Because of the shorter Pt–Pt distance compared to the Pt(1)–Pt(2) distance in the tetramer, the transition should shift to higher energy and the transition moment should increase. Both of these factors contribute to increasing the oscillator strength of the transition in the Pt dimer and could lead to the observed increase in energy and intensity of the 480-nm band.

Compared to the *z*-polarized bands at 680 and 480 nm, the three *x*-polarized absortions are weak; the strongest of them occurs at 460 nm[26] and corresponds to the transition from orbital 26 $b_g\downarrow$

(25) The lowest energy dipole-allowed spin-forbidden transition, 31 b_u (^2B_u) → 33 a_g(^4A_g), is predicted at 3.12 eV. Spin-forbidden transitions are therefore not expected to contribute to the observed spectrum, except possibly for the 400-nm band.

Table IV. Orbitals with Significant Pt–Pt Interaction

orbital	interaction	comment
32 b_u ↑ (HOMO)	Pt(1)–Pt(2) and Pt(2)–Pt(2) σ^*	strong, partly cancels 23 a_g
31 a_g ↓	Pt(1)–Pt(2) antibonding and Pt(2)–Pt(2) bonding	weak
30 a_g ↓ 30 a_g ↑	Pt(1)—Pt(2) antibonding and Pt(2)–Pt(2) bonding	weak
27 b_g ↓ 27 b_g ↑	Pt(1)–Pt(2) and Pt(2)–Pt(2) π^*	weak, cancels 25 a_u
29 b_u ↓ 29 b_u ↑	Pt(2)–Pt(2) δ^*	weak, cancels 29 a_g
29 a_g ↓ 29 a_g ↑	Pt(2)–Pt(2) δ	weak, cancels 29 b_u
28 a_g ↓ 28 a_g ↑	Pt(1)–Pt(2) σ^* and Pt(2)–Pt(2) σ	medium, cancels 25 b_u
27 a_u ↓ 27 a_u ↑	Pt(1)–Pt(2) π^* and Pt(2)–Pt(2) π	weak, cancels 25 b_g
28 b_u ↓ 28 b_u ↑	Pt(1)–Pt(2) π^* and Pt(2)–Pt(2) π	weak, cancels 27 a_g π
25 b_g ↓ 25 b_g ↑	Pt(1)–Pt(2) π and Pt(2)–Pt(2) π^*	weak, cancels 27 a_u
27 a_g ↓ 27 a_g ↑	Pt(1)–Pt(2) π	weak, cancels 28 b_u π^*
26 b_u ↓ 26 b_u ↑	Pt(1)–Pt(2) and Pt(2)–Pt(2) π	weak
25 a_u ↓ 25 a_u ↑	Pt(1)–Pt(2) and Pt(2)–Pt(2) π	weak, cancels 27 b_g
25 b_u ↓ 25 b_u ↑	Pt(1)–Pt(2) σ and Pt(2)–Pt(2) σ^*	medium, cancels 28 a_g
23 b_u ↓ 23 b_u ↑	Pt(1)–Pt(2) σ and Pt(2)–Pt(2) σ^*	medium
23 a_g ↓ 23 a_g ↑	Pt(1)–Pt(2) and Pt(2)–Pt(2) σ	strong, cancels 32 b_u ↑

Table V. Electronic Absorptions and Assignments for $[Pt(NH_3)_2(C_5H_4NO)]_4^{5+}$

obsd values					
λ_{max}, nm	energy, eV	polarization and intensity	C_{2h} transition[a]	calcd energy, eV	predicted[b,c] polarization and intensity
			32 a_g (^2B_u) → 32 b_u (^2A_g)	0.48[d]	(y,z); w
			28 b_g (^2B_u) → 32 b_u (^2B_g)	0.75[d]	(x); w
~800[g]	~1.55	(?); vw	27 b_g (^2B_u) → 32 b_u (^2B_g)	1.63[d]	(x); w
			31 a_g (^2B_u) → 32 b_u (^2A_g)	1.50[d]	(y,z); s
680	1.82	(z); s, br[f]	30 a_g (^2B_u) → 32 b_u (^2A_g)	1.53[d]	(y,z); s
			29 a_g (^2B_u) → 32 b_u (^2A_g)	1.86[e]	(y,z); w
			28 a_g (^2B_u) → 32 b_u (^2A_g)	2.14[d]	(y,z); s
			28 b_u (^2B_u) → 32 b_u (^2B_u)	2.15[d]	(x); vw
550	2.25	(x); vw	27 a_u (^2B_u) → 32 b_u (^2A_u)	2.16[d]	(x); vw
			26 a_u (^2B_u) → 32 b_u (^2A_u)	2.39[d]	(x); vw
480	2.58	(z); m	27 a_g (^2B_u) → 32 b_u (^2A_g)	2.80[e]	(y,z); s
			32 b_u (^2B_u) → 33 a_g (^2A_g)	2.96[e]	(y,z); ?
			26 a_g (^2B_u) → 32 b_u (^2A_g)	3.05[d]	(y,z); w
460	2.69	(x); wm	26 b_g (^2B_u) → 32 b_u (^2B_g)	2.39[d]	(x); m
400	3.10	(x); w	25 b_g (^2B_u) → 32 b_u (^2B_g)	2.84[e]	(x); w
			32 b_u (^2B_u) → 29 b_g (^2B_g)	3.10[d]	(x); w

[a] Dipole and spin-allowed transitions below 3.0 eV. The transitions assigned to the 550-nm band are dipole-forbidden, vibronically-allowed. [b] The "predicted intensity" is a qualitative estimate of the transition moment (see text). [c] Abbreviations: v = very, s = strong, m = medium, w = weak, br = broad. [d] Ground-state energy level difference with average relaxation correction. [e] Spin-unrestricted transition-state energy. [f] A weak x-polarized 680-nm band is also observed. This is attributed to the same transition as the strong z-polarized band—see discussion in text. [g] Observed only in the diffuse reflectance spectrum.

to the LUMO. Orbital 26 b_g has 31% of its charge on the pyridone nitrogen atoms, with the remainder of the charge largely on the pyridone ring carbon atoms. The transition owes its intensity to the components N(3) p → Pt(1) $d_{z^2}^-$, d_{yz}^- and may be described as pyridone nitrogen-to-platinum charge transfer. On the pyridone nitrogen the charge is associated with a p_z, p_y, p_x hybrid basis function which is poorly oriented for strong interaction with either Pt(1) $d_{z^2}^-$ or Pt(1) d_{yz}^-; the resulting charge-transfer band is therefore weak. After the 460-nm band, the most intense x-polarized absorption occurs at 400 nm. It corresponds to one or both

of the transitions 25 $b_g\downarrow \rightarrow$ 32 $b_u\downarrow$ and 32 $b_u\downarrow \rightarrow$ 29 $b_g\downarrow$ (Table V) and owes its intensity to d–d component transitions on Pt(1) and Pt(2).

There remain to be assigned two very weak absorptions: an *x*-polarized band at 550 nm and a feature of unknown polarization at ~800 nm (diffuse reflectance spectrum). Only one dipole-allowed transition below 3.0 eV has not been accounted for; we assign the ~800-nm feature to this transition since it is in good agreement with the predicted energy (Table V).[27] The 550-nm band must be attributed to dipole-forbidden vibronically allowed transitions. There are three transitions of this type which are in good agreement with the observed energy (Table V). Since the 550-nm band is observed only below 30 K, the vibronic coupling presumably occurs in the excited state and causes its symmetry to become ^2B_g. Mixing of this state with the nearby ^2B_g state associated with the 26 $b_g\downarrow \rightarrow$ 32 $b_u\downarrow$ transition transfers intensity from the 460-nm dipole-allowed ligand-to-metal charge-transfer band to the 550-nm band.

Discussion of Other Spectroscopic Results and Chemical Behavior. XPS,[5b] ESR,[5c,d] and the present single-crystal optical spectroscopic measurements indicate that the unpaired spin in *cis*-diammineplatinum α-pyridone blue is in a d_{z^2}-like molecular orbital delocalized over the Pt chain. This conclusion is confirmed by the Xα calculation which shows the PPB HOMO to be delocalized over all four Pt atoms and to be comprised of overlapping $d_{z^2}^-$, d_{yz}^-, p_z^+ hybrid orbitals on Pt(1) and $d_{z^2}^-$, s^- hybrid orbitals on Pt(2). Of the unpaired spin density 91% is contained within the Pt spheres, with 41% in 2 Pt(1) and 50% in 2 Pt(2). PPB is evidently a Robin–Day class III-A compound.[28,29]

Since the Xα calculation has provided a description of the valence MO's of PPB, we can now rationalize certain aspects of its behavior and point out some interesting possibilities which have not yet been realized. Addition of an electron to the σ* LUMO is expected to cancel the Pt(2)–Pt(2) bond. This expectation is realized through the observation that the one-electron reduction product of PPB is a Pt(II) dimer which associates in the solid state to a tetramer with a nonbonding Pt(2)–Pt(2) interaction.[23] Electron donation by axial ligands and excitation by light can also increase the electron density in the LUMO and promote dissociation of the Pt(2.25) tetramer to dimers. The effectiveness of donor anions in causing the dissociation of the tetramer has been observed,[5d] but the effect of light has not been studied. Removal of an electron from the PPB HOMO is expected to increase the strength of both Pt(1)–Pt(2) and Pt(2)–Pt(2) bonding. A one-electron oxidation of PPB should therefore lead to a Pt(2.5) tetramer. This species has not yet been observed since in the experiments where oxidation was carried out it is likely that the tetramer was largely predissociated.[23] A tetranuclear Pt(2.5) α-pyridone analogue, $[Pt(NH_3)_2(C_4H_6NO)]_4^{6+}$ (C_4H_6NO = α-pyrrolidonate), is known,[3d] however, and has Pt–Pt distances of 2.70 Å, ca. 0.15 Å shorter than in PPB. Further successive one-electron oxidations of **a** Pt(2.5) tetramer to Pt(2.75) and Pt(III) tetramers would also appear to be possible. The electrons for these oxidations would be removed from orbital 32 a_g. Since orbital 32 a_g does not show metal–metal interaction but is Pt–pyridone oxygen π* in character, it is expected that Pt(2.5), Pt(2.75), and Pt(III) tetramers would all have similar metal–metal bonding but that the Pt(2.75) and Pt(III) complexes would have slightly shorter Pt–pyridone oxygen bonds.[30]

Acknowledgment. This work was supported by PHS Grants CA 15826 (at Columbia University) and CA 34992 (at MIT) awarded by the National Cancer Institute (to S.J.L.), DHHS, and at the University of Kentucky by a grant from the Research Corporation (to P.E.F.). We thank Engelhard Industries for a generous loan of K_2PtCl_4 from which the platinum compound was synthesized.

Registry No. PPB, 62782-86-9.

Supplementary Material Available: Table S1 reporting the atomic coordinates, sphere radii, and α values used in the calculation, Tables S2–S3 reporting valence and core levels, and Table S4 reporting virtual levels (18 pages).

(26) Some of the intensity underlying the 460-nm (*x*) band must be due to the forbidden *x* component of the 480-nm (*y*,*z*) band, which should become manifest by the same mechanisms discussed earlier for the *x* component of the 680-nm (*y*,*z*) band. It is unlikely that this could account for more than half of the observed intensity.

(27) It may be that the ~800-nm feature is an artifact and that the 27 $b_g\downarrow \rightarrow$ 32 $b_u\downarrow$ transition is not observed. We reject assigning this transition to the 550-nm band because of the large discrepancy between calculated and observed energy.

(28) Robin, M. B.; Day, P. *Adv. Inorg. Chem. Radiochem.* **1967**, *10*, 247.

(29) Wong, K. Y.; Schatz, P. N. *Prog. Inorg. Chem.* **1981**, *28*, 369.

(30) *cis*-Diammineplatinum(III) dimers with bridging α-pyridonate ligands have Pt–O distances[23] of 1.991–2.007 Å compared to 2.016 and 2.022 Å in PPB.

Theoretical Study of Dimeric Forms of Ground-State Benzene Molecules[1a]

Ray Engelke, P. Jeffrey Hay,* Daniel A. Kleier,[1b] and Willard R. Wadt

Contribution from Los Alamos National Laboratory, Los Alamos, New Mexico 87545.
Received October 20, 1983

Abstract: The relative energies and interconversion barriers of four chemically bound dimeric forms of benzene—*p*,*p*′-dibenzene (**2**), hexaprismane (**3**), and *exo*- and *endo*-*o*,*o*′-dibenzene (**4** and **5**)—are examined by using semiempirical MNDO calculations, ab initio GVB–CI techniques, and thermochemical group-additivity methods. We conclude from the calculations that the relative energies of these species are **3** > **4**, **5** > **2** > two benzene molecules (**1**). The species **2** and **3** are metastable along D_{2h} pathways; the decomposition **2** → **1** is also found to have a large energy barrier along a C_{2v} pathway. Similar conclusions are found for the reactions **4** → **1** and **5** → **1** along C_{2h} and C_{2v} paths. Of the species examined only **5** has been observed in the laboratory. Previous efforts to produce the dimers experimentally are briefly discussed.

Of the various chemically bound $(CH)_{12}$ isomers that could be formed from two ground-state benzene molecules (**1**), possibilities include the *p*,*p*′-dibenzene (**2**) and *o*,*o*′-dibenzene (**4** and **5**) species and the highly strained hexaprismane (**3**) molecule. Of these

0002-7863/84/1506-5439$01.50/0